ADVANCED FUNCTIONAL MATERIALS

Controlling Steps During Early Stages of the Aligned Growth of Carbon Nanotubes Using Microwave Plasma Enhanced Chemical Vapor Deposition**

By *Li-Chyong Chen*,* *Cheng-Yen Wen*, *Chi-Huei Liang*, *Wei-Kai Hong*, *Kuo-Ji Chen*, *Huang-Chung Cheng*, *Ching-Shing Shen*, *Chien-Ting Wu*, and *Kuei-Hsien Chen*

Vertically aligned carbon nanotubes (CNTs) with controllable length and diameter fabricated by microwave plasma enhanced chemical vapor deposition (MPECVD) are of continuing interest for various applications. This paper describes the role of process gas composition as well as the pre-coating catalytic layer characteristics. It is observed that nucleation of CNTs was significantly enhanced by adding nitrogen in the MPECVD process, which also promoted formation of bamboo-like structures. The very first key step toward growth of aligned CNTs was the formation of high-density fine carbon onion encapsulated metal (COEM) particles under a hydrogen plasma. Direct microscopic investigation of their structural evolution during the very early stages revealed that elongation, necking, and splitting of the COEM particles occurred accompanying the growth of CNTs, such that one of the split portions rode on the top of the growing tube while the remaining one resided on the root. Our results suggest that CNTs grow via the "tip-growth" as well as "root-growth" mechanisms.

1. Introduction

Material preparation, characteristic properties, and device fabrication are often intertwined in the development of nanoscience and nanotechnology. A remarkable example is the newly discovered carbon nanotube (CNT), which exhibits extremely high emission currents at very low operating voltage unmatched by other materials.[1–9] Despite the fact that the work function of CNTs is high, the exceptionally large field enhancement resulting from the sharp curvature of CNTs is one of the key factors responsible for their low threshold field. In addition, the higher electron conductivity of CNTs is also advantageous for drawing higher emission currents. Prototypes of cathode-ray-tube lighting elements[10] and 4.5 inch (1 inch ≈ 2.5 cm) CNT field-emission displays[11] have been demonstrated. However, despite the initial promise of CNTs transfer to practical cathode applications has been impeded partly due to the lack of strategies in large-scale growth of CNTs and process integration of CNTs with other components. In some devices CNTs with stringent quality requirements, such as being defect-free, might be essential. In other devices CNTs with good orientation alignment and length control are desirable.[12–15] Additional geometric factors such as the number density, the size, and aspect ratio of the nanotubes can also affect the overall emission characteristics.[16,17] Therefore, it is imperative to understand the key steps for aligned growth with size specificity.

Among the process techniques, conventional thermal chemical vapor deposition (CVD) has been successfully employed for self-oriented growth of CNTs,[7] whereas plasma-enhanced CVD has gained increasing popularity as a controllable and deterministic method for growing vertically aligned CNTs.[5,12–15,17–24] Although it is now relatively easy to generate aligned CNTs, the key steps that control the aligned growth of the CNTs are still an open question. Without using any template or substrate with confined geometric features, applying extra bias during growth was found to be effective for controlling the orientation of CNTs.[20,22] Meanwhile, Bower et al. proposed that the alignment of CNTs grown by microwave-plasma-enhanced chemical vapor deposition (MPECVD) is primarily induced by the electrical self-bias imposed on the substrate surface from the microwave plasma.[24]

In this paper, we attempt to address several issues pertaining to the aligned growth of CNTs by MPECVD. Specifically, we use both field-emission scanning electron microscopy (FESEM) and high-resolution transmission electron microscopy (HRTEM) to study the microstructure evolution of the CNTs at the very initial stages. It should be emphasized that our synthetic approach is simple and straightforward, in that it only involves the MPECVD process using Si substrates that are precoated with a thin layer of Fe, Ni, or Co metals. Pretreatment of the catalytic metal, such as exposure to NH_3 gas[5] or dipping in HF solution,[25] was not required. Besides, there was no extra bias during the MPECVD growth process. However, we find

[*] Dr. L. C. Chen, C. Y. Wen, C. H. Liang
Center for Condensed Matter Sciences, National Taiwan University
1 Roosevelt Road, Section 4, 106, Taipei (Taiwan)
E-mail: chenln@ccms.ntu.edu.tw
W. K. Hong, K. J. Chen, Prof. H. C. Cheng
Department of Electronics Engineering and Institute of Electronics
National Chiao Tung University
1001 Tashuei Road, 300, Hsinchu (Taiwan)
C. S. Shen, C. T. Wu, Dr. K. H. Chen
Institute of Atomic and Molecular Sciences, Academia Sinica
P.O. Box 23-166, 106, Taipei (Taiwan)

[**] The authors acknowledge financial support for this project from the National Science Council (NSC) in Taiwan under contract nos. NSC 89-2112-M-002-085 and NSC90-2112-M-002-048 as well as from the Ministry of Education in Taiwan under contract no. 89-W-FA01-2-4-5.

  1616-301X/02/1010-0687 $ 17.50+.50/0

that self-bias alone is not sufficient for aligned growth. Other process parameters, such as the process gas composition as well as the pre-coating catalytic layer crystallinity and layer thickness, also have a strong effect on the resultant morphology. Interestingly, the formation of carbon onion encapsulated metal (COEM) particles during H-plasma treatment turns out to be a crucial intermediate step for further growth of CNTs. Furthermore, observation of the structural evolution of CNTs in the early stages has provided direct evidence, for the first time, of dual growth mechanisms, namely, tip-growth and root-growth, which occur simultaneously in the formation of CNTs.

Aligned carbon nanotubes can be synthesized by MPECVD with a rather wide range of process parameters on metal catalyst layers prepared by e-beam evaporation on Si substrate. The most critical parameters are the metal layer thickness, hydrogen plasma pretreatment, gas composition, and the substrate temperature. Depending on the specific process parameters, the resultant microstructure can be quite different. In the following we describe comparative investigations of a few parameters that generate pronounced structure differences. In particular, characteristic features that are related to the formation of aligned CNTs will be emphasized. Furthermore, microstructure evolution during the very early stages of growth was monitored in detail.

2. Effects of N_2 Addition

Figure 1 shows the cross-sectional SEM images of CNT samples synthesized using different gas mixtures but otherwise identical deposition parameters. Both samples were deposited on Si substrates pre-coated with an e-beam evaporated Fe layer 7 nm thick, as determined from cross-sectional TEM images. It can be seen that the CNT sample prepared using a CH_4/H_2 gas mixture showed a spaghetti-like morphology (Fig. 1a), while its counterpart prepared with nitrogen addition exhibited vertical alignment of the CNTs (Fig. 1b). The mechanism of the aligned growth is mainly attributed to the high density of CNTs being grown from the densely packed catalytic nanoparticles. As the nanotubes lengthen, they interact with nearby nanotubes, presumably by van der Waals forces, to form a large bundle with some rigidity, which enables them to keep growing along the same direction.

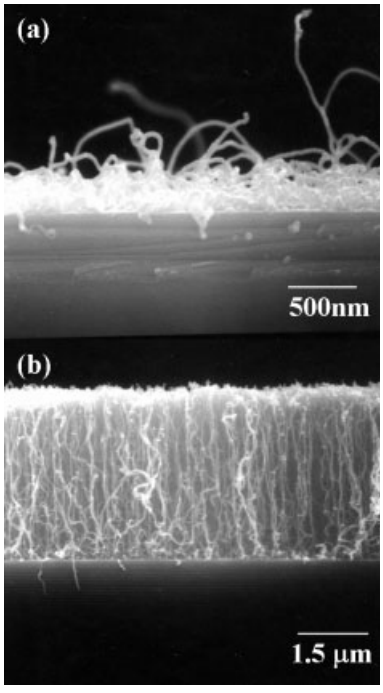

Fig. 1. Cross-sectional SEM images of CNTs grown by MWCVD on Fe-coated Si substrates, with a Fe-layer thickness of 7 nm. a) CH_4/H_2 = 20:80 sccm and b) $CH_4/H_2/N_2$ = 20:80:80 sccm. Other process parameters are identical: microwave power 1500 W, chamber pressure 6.6 kPa, substrate temperature 680 °C, and growth time 20 min.

Figure 2 shows the HRTEM images corresponding to those shown in Figure 1. The sample prepared with a CH_4/H_2 gas mixture exhibited a typical multi-wall carbon nanotube structure (Fig. 2a), whereas the majority of the CNTs found in the sample prepared with N_2 addition showed bamboo-like structure (Fig. 2b). It is also noted that the average diameter of the former sample, i.e., the CNT prepared without N_2 addition, was usually smaller than that of the latter one. Furthermore, the CNTs only contained a couple of walls in the tube, especially when a CH_4/Ar-based gas mixture was used. However, single-wall CNTs were rarely observed in the present process.

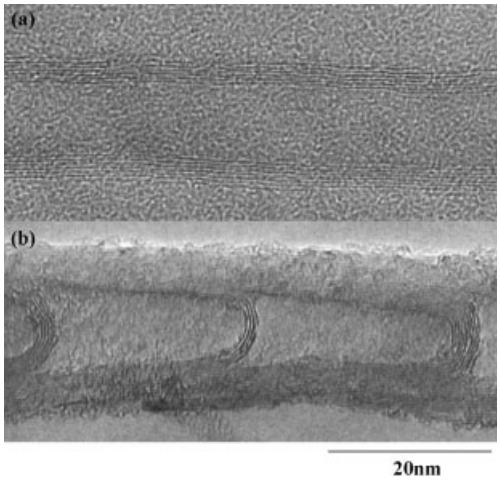

Fig. 2. HRTEM images of the Fe-catalyzed CNTs grown with a gas mixture of a) CH_4/H_2 and b) $CH_4/H_2/N_2$. These two samples are the same as those shown in Figure 1. The CNTs prepared with N_2 addition exhibit bamboo-like structure.

Thus, the addition of N_2 in the process gas not only enhances the nucleation of the CNTs, but also promotes the formation of bamboo-like structure. Consistent with the observation by Cui et al. in a similar process,[26] the inter-bamboo node distance also decreases with increasing N/C ratio in the process gas. This suggests that the nitrogen or its active gaseous species in the microwave plasma might assist the formation of a high curvature surface. This can be intuitively understood, since the bonding of the nitrogen atom in a solid-state network is inherently non-planar with the presence of a lone pair of electrons, whereas the sp^2 bonding of the carbon atom is usually planar. It should be mentioned that some incorporation of nitrogen in the CNTs was observed by Auger electron spectroscopy

  1616-301X/02/1010-0688 $ 17.50+.50/0

ADVANCED FUNCTIONAL MATERIALS

(AES), when the sample was deposited with N_2 addition. The level of nitrogen incorporation increased only slightly with an increasing fraction of N_2 in the process gas. However, only up to about 8 at.-% of N in CNTs was detected by AES.

3. Effects of Catalyst Layer Thickness

Figures 3 and 4 show the SEM images of CNTs grown on Fe- and Co-coated Si substrates, respectively, with various catalyst layer thicknesses. Except for the catalyst material and layer thickness, all the samples were grown under the same conditions, namely, $CH_4/H_2/N_2$ = 20:80:80 sccm, microwave power 1500 W, chamber pressure 6.6 kPa, substrate temperature 680 °C, and growth time 10 min. It is quite clear that, regardless of the type of catalyst material, the thicker the catalyst layer, the larger the average diameter of the CNTs. Pure CNTs could be grown uniformly over the entire substrate with a catalyst layer thickness between 3 and 50 nm. Outside this range mixed phases and/or graphitic balls were formed. It should be emphasized that, in fact, hydrogen plasma treatment of the catalyst prior to the growth of CNTs is critical to the growth and size control of the CNTs. Without this treatment, mixed carbonaceous deposits instead of pure CNTs were formed. As will be demonstrated in this section, the hydrogen plasma treatment not only cleans the surface of the catalyst layer but also produces a more active catalyst morphology.

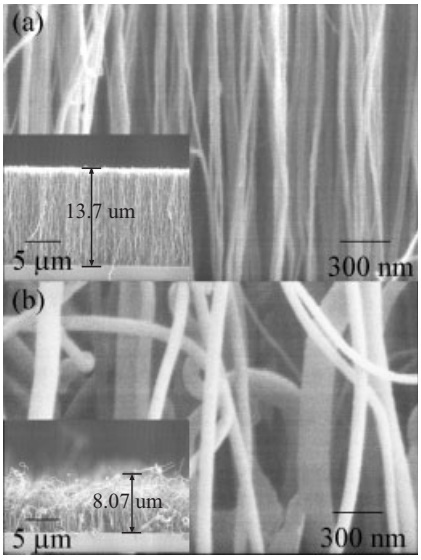

Fig. 3. Cross-sectional SEM images of CNTs grown on a Fe-coated Si substrate with a Fe-layer thickness of a) 3.5 nm and b) 15 nm, but otherwise identical process parameters as for the sample shown in Figure 1b. The insets were taken at lower magnification to show the length of the CNTs.

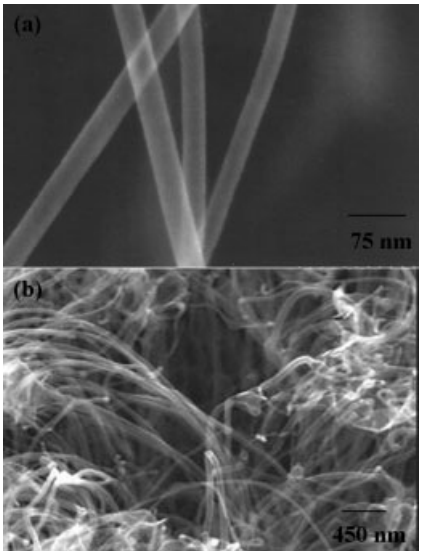

Fig. 4. Cross-sectional SEM images of CNTs grown on a Co-coated Si substrate with a Co-layer thickness of a) 7 nm and b) 30 nm, but otherwise identical process parameters as for the sample shown in Figures 1b and 3.

Investigation of the sample right after hydrogen plasma treatment, at 80 sccm H_2 flow rate and 1000 W microwave power for 10 min, revealed that the catalyst layer had been transformed into nanoparticles. Figure 5 depicts the cross-sectional HRTEM image of a Fe-coated Si substrate that has been subjected to hydrogen plasma treatment. The 7 nm Fe thin film was transformed into densely distributed and yet well-separated Fe particles 10–20 nm in diameter. It should also be noted that carbon onions encapsulated these metal nanoparticles. Without introducing any external carbon source at this H-plasma-treatment stage, the observed carbon onions were likely to form during preparation of the TEM samples. However, residual carbon in the chamber cannot be ruled out for the in-situ formation of the carbon onion encapsulating metal particles (COEM).

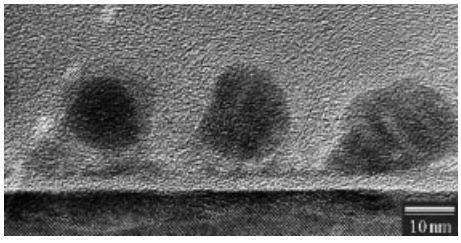

Fig. 5. Cross-sectional HRTEM image of a Si substrate with an Fe coating of 7 nm that was only subjected to H_2 plasma treatment at 1 kW for 10 min. At this stage, carbon onion encapsulated metal (COEM) particles formed.

Figures 6 and 7 show the SEM images of various Fe layer coated Si substrates that have been subjected to H_2 plasma treatment. The average size of the COEM particles increased with the catalyst layer thickness. The size of the COEM particles, which can be conveniently controlled by the film thickness, is a decisive factor for morphological control of the CNTs. A strong correlation of the diameter of the CNTs with the size of the dispersed metal particles has also been reported by other research groups.[20,27] As evident from the inserts shown in Figure 3, the thinner catalyst layer not only leads to CNTs with smaller diameter but also results in apparently longer CNTs than its thicker counterpart. Be it tip growth or root growth, carbon species produced by the adsorption and decomposition of CH_4 on the surface of catalyst nanoparticles must diffuse around the surface of the nanoparticles and/or through the bulk of the nanoparticles to form a CNT. Presumably, the larger nanoparticles derived from thicker catalyst layers had a

  1616-301X/02/1010-0689 $ 17.50+.50/0

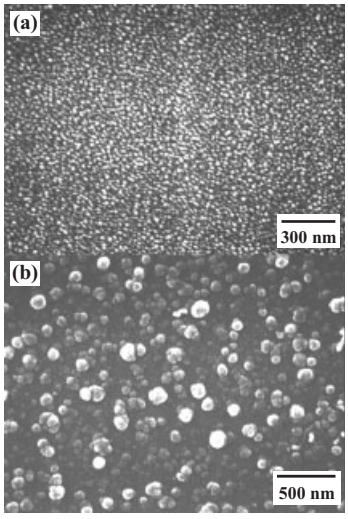

Fig. 6. SEM (top view) images of 3.5 nm (a) and 15 nm (b) Fe-layer coated on a Si substrate after H_2 plasma treatment at identical conditions as for the sample shown in Figure 5. The average size of the COEM particles is correlated to the layer thickness of the Fe coating.

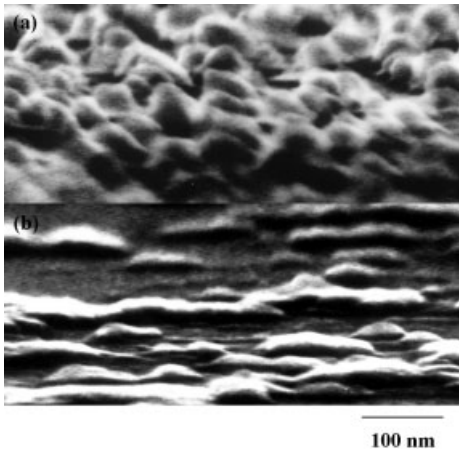

Fig. 7. SEM (tilted view) images of a 7 nm (a) and 30 nm (b) Fe-layer coated on a Si substrate after H_2 plasma treatment at identical conditions as for the sample shown in Figures 5 and 6.

smaller surface-to-volume ratio, which therefore led to a longer reaction time to achieve the same growth condition. We also observed that the Fe-catalyzed CNTs exhibited a better vertical alignment than their Ni- and Co-catalyzed counterparts. However, the origin of this difference is unclear.

4. Structural Evolution of the CNT

The formation of metal nanoparticles under hydrogen plasma treatment is a crucial step for subsequent growth of the CNTs. Once these nanoparticles were formed, growth of CNTs occurred rapidly with negligible incubation time at the moment of introducing methane and nitrogen into the reactor. In this section we present FESEM and HRTEM investigations on the structural evolution of CNTs during the early stages of growth. Except for the growth time, this series of samples was grown at identical conditions, i.e., $CH_4/H_2/N_2$ = 20:80:80 sccm, microwave power 1500 W, chamber pressure 6.6 kPa, substrate temperature 680 °C. Figure 8 depicts a typical FESEM image of a sample grown for only 10 s. Some CNTs (~15 nm) were visible even at this very initial stage of growth.

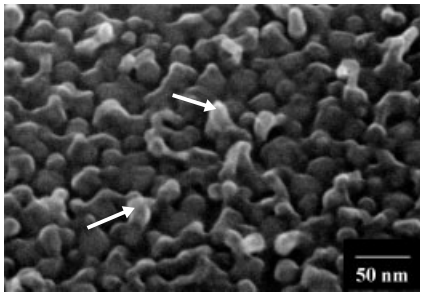

Fig. 8. FESEM image of CNTs grown for only 10 s on a Fe-coated Si substrate with a Fe-layer thickness of 7 nm. Except for the growth time, all process parameters are identical to the ones for the sample shown in Figure 1b. Initial growth of some CNTs is indicated by arrows.

After a process time of 40 s, the CNTs had already grown to a substantial length (~400 nm) and uniformly covered the entire substrate. Typical top view and cross-sectional view FESEM images of this 40 s sample are shown in Figures 9 and 10, respectively. Both the secondary electron image (SEI) and back-scattering electron image (BEI) are depicted. The SEI gives mostly geometric contrast, while the BEI reveals enhanced atomic contrast. The larger the atomic number, the brighter it appears in the BEI. Thus the bright regions in the BEI are attributed to Fe whereas C gives very little signal. Due to the large atomic number difference between Fe and C, the BEI can be quite distinct, as exemplified in both Figures 9b and 10b, from the SEI wherein CNTs dominate the morphology. The Fe nanoparticles that can be clearly seen from Figure 9b were uniformly distributed with a rather narrow size distribution. As is also evident from Figure 10b, the BEI revealed that the catalysts resided both at the roots and at the

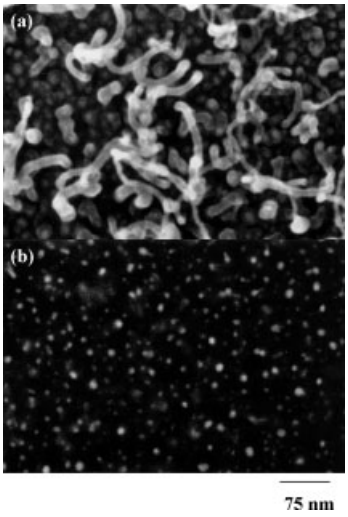

Fig. 9. Top view FESEM images of CNTs grown for only 40 s on an Fe-coated Si substrate with a Fe-layer thickness of 7 nm taken in a) secondary electron imaging (SEI) mode and b) backscatter electron imaging (BEI) mode. Except for the growth time, all process parameters are identical to the ones for the sample shown in Figures 1b and 8.

  1616-301X/02/1010-0690 $ 17.50+.50/0

ADVANCED FUNCTIONAL MATERIALS

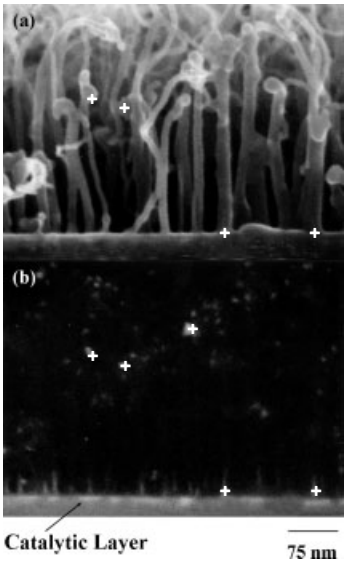

Fig. 10. Cross-sectional FESEM images of CNT samples corresponding to those shown in Figure 9 taken in a) SEI mode and b) BEI mode. The crosses indicate the identical pairs of points of the sample in the SEI and BEI modes. The arrow indicates the catalytic layer.

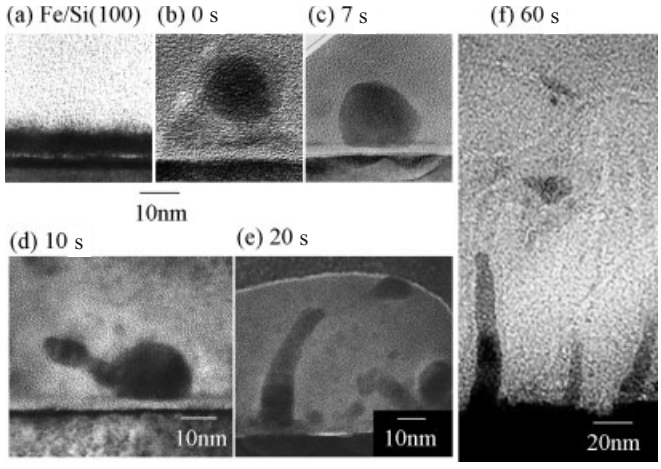

Fig. 11. Cross-sectional HRTEM images showing microstructural evolution of the CNTs at the early stages of growth: a) as-deposited Fe layer (7 nm) on a Si substrate, b) after H-plasma treatment only, i.e., 0 s of growth, c) 7 s of growth, d) 10 s of growth, e) 20 s of growth, and f) 60 s of growth. Growth parameters are the same as for the sample shown in Figure 1b.

tips. This observation is intriguing and contrary to literature data where the catalyst nanoparticles were reported either at CNTs tips only or at the roots only. Previous studies on the CVD growth of CNTs suggested a mechanism quite similar to that reported for carbon fiber: first, diffusion of carbon occurs through the bulk and/or on the surface of the catalytic particles. It is followed by precipitation of carbon from supersaturated transition metal particles.[28–30] In such a process, a temperature gradient is formed and the carbon fiber precipitates from the cooler end of the particle. Thus, depending on the bonding between the catalyst and the substrate, a "tip-growth" or "root-growth" mechanism was proposed accordingly. Invariably it is a resurrected issue of controversy whenever any catalyst assisted method of CNT growth is reported.

We propose that both "tip-growth" and "root-growth" mechanisms can operate simultaneously in the present case. Cross-sectional HRTEM investigations on the structural evolution during the first minute of CNT growth are shown in Figure 11. As described before, the 7 nm Fe thin film (Fig. 11a) was transformed into nanoparticles (Fig. 11b) after hydrogen plasma treatment. Then, a continuous thickening of the carbon onions occurred immediately after introducing CH_4 and N_2 (Fig. 11c). Within 10 s of growth, the carbon onion-encapsulated Fe particles became unstable, presumably due to the large curvature of the graphite layer. With further supply of active carbon source, this instability induced a transformation of the carbon onions into carbon nanotubes. Accompanying the formation of carbon nanotubes, elongation, necking, and splitting of the Fe particles was observed after 10 s of growth (Figs. 11d–f). As clearly shown in Figure 11e, splitting of the elongated catalyst into two droplets occurred inside the same tube and one of the split droplets was raised along with the tip of the CNT. Within less than a minute, the CNT structure was already fully developed. Thereafter, most of the tips encapsulating Fe droplets were far away from the tube–substrate interface leaving only the cone-shaped Fe in the roots of the tubes within the field of imaging (Fig. 11f).

Figure 12 shows the cross-sectional SEM images of the samples prepared with growth times from 3 to 20 min. The length of the CNTs increased quite rapidly during the first 10 min of the growth, while the diameter of the tubes remained fairly constant. The growth rate of the CNTs was about 400 nm per minute at the initial stage and leveled off after 20 min for the experimental runs with the conditions described earlier. The mechanism causing the saturation in the growth remains to be verified. By comparing the length evolution of the CNTs grown at various temperatures, the initial growth rate clearly increased with the growth temperature, suggesting a thermally activated process. However, the nonlinear behavior of the length versus growth time implied that this process could not be simply described by a single activation energy. A more detailed study is needed to resolve the controlling growth mechanism of CNTs at different stages.

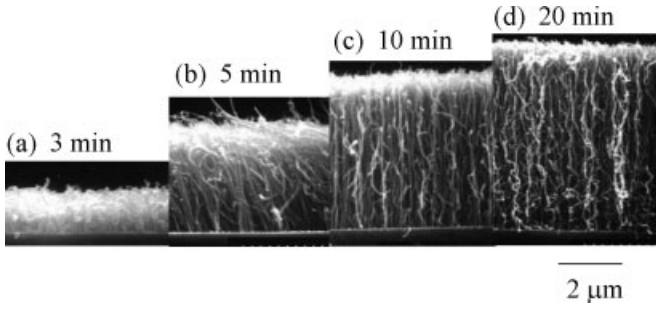

Fig. 12. Cross-sectional SEM images showing microstructural evolution of the CNTs at the later stages of growth: a) 3 min, b) 5 min, c) 10 min, and d) 20 min. Growth parameters are the same as for the sample shown in Figure 1b.

  1616-301X/02/1010-0691 $ 17.50+.50/0

5. Conclusions

Well-aligned carbon nanotubes were grown perpendicular to the surface of Fe- and Co-coated Si substrates by microwave plasma enhanced chemical vapor deposition in mixtures of CH_4, N_2, and H_2 with various flow rates. Nitrogen addition not only promoted the formation of bamboo-like structures but also significantly enhanced nucleation of CNTs, leading to orientational alignment mainly through a crowding effect. Formation of high-density fine carbon onion encapsulated metal particles was observed under hydrogen plasma treatment. The thickness of the catalytic layer controlled the size of the COEM particles, which in turn determined the diameter of the CNTs. Growth of CNTs initially occurred rapidly and within minutes thereafter it exhibited a saturation behavior. Detailed microscopy observations revealed that elongation, necking, and splitting of the COEM particles occurred accompanying the growth of CNTs, suggesting that CNTs grow via both the "tip-growth" as well as "root-growth" mechanism.

6. Experimental

Metal layers with various thickness were deposited on Si substrates by electron beam evaporation. Afterwards, the CNTs were grown on the pre-coated Si substrates by MPECVD. The experiments were performed with microwave power ranging from 1 to 2 kW. For any given microwave power, the chamber pressure was adjusted such that the plasma was most stable. By varying the microwave power, the substrate temperature can be varied between 500–1000 °C. The actual substrate temperature during CNT growth was measured by an optical pyrometer. Mixtures of CH_4, N_2, and H_2 with various flow rates were used as the source gases. The deposition time was varied between 10 s and several minutes. Prior to CNT growth, hydrogen plasma treatment (1 kW, 10 min) was employed for cleaning the substrate and forming the COEM particles. It should be mentioned that the coated substrate was covered with an additional Si wafer to avoid direct exposure to the plasma. Without the shielding, the CNTs cannot be formed. A detailed discussion of this aspect will be published in a separate paper. For microstructure investigation, a JEOL 6700, a Hitachi S-5000 FESEM and a Philips CM200 HRTEM were used.

Received: December 21, 2001
Final version: May 15, 2002

[1] W. A. de Heer, A. Chatelain, D. Ugarte, *Science* **1995**, *270*, 1179.
[2] P. G. Collins, A. Zettl, *Appl. Phys. Lett.* **1996**, *69*, 1969.
[3] Y. Saito, K. Hamaguchi, T. Nishino, K. Uchida, Y. Tasaka, F. Ikazaki, M. Yumura, A. Kasuya, Y. Nishina, *Nature* **1997**, *389*, 554.
[4] Q. H. Wang, T. D. Corrigan, J. Y. Dai, R. P. H. Chang, A. R. Krauss, *Appl. Phys. Lett.* **1997**, *70*, 3308.
[5] Z. F. Zen, Z. P. Huang, J. W. Xu, J. H. Wang, P. Bush, M. P. Siegal, P. N. Provencio, *Science* **1998**, *282*, 1105.
[6] J.-M. Bonard, J. Salvetat, T. Stockli, W. A. de Heer, L. Forro, A. Chatelain, *Appl. Phys. Lett.* **1998**, *73*, 918.
[7] S. Fan, M. G. Chapline, N. R. Franklin, T. W. Tombler, A. M. Cassell, H. Dai, *Science* **1999**, *283*, 512.
[8] W. Zhu, C. Bower, O. Zhou, G. Kochanski, S. Jin, *Appl. Phys. Lett.* **1999**, *75*, 873.
[9] F. G. Tarntair, L. C. Chen, S. L. Wei, W. K. Hong, K. H. Chen, H. C. Cheng, *J. Vac. Sci. Technol. B* **2000**, *18*, 1207.
[10] Y. Saito, S. Uemura, K. Hamaguchi, *Jpn. J. Appl. Phys.* **1998**, *37*, L346.
[11] W. B. Choi, D. S. Chung, J. H. Kang, H. Y. Kim, Y. W. Jin, I. T. Han, Y. H. Lee, J. E. Jung, N. S. Lee, G. S. Park, J. M. Kim, *Appl. Phys. Lett.* **1999**, *75*, 3129.
[12] H. C. Cheng, W. K. Hong, F. G. Tarntair, K. J. Chen, J. B. Lin, K. H. Chen, L. C. Chen, *Electrochem. Solid-State Lett.* **2001**, *4(4)*, H5.
[13] H. C. Cheng, K. J. Chen, W. K. Hong, F. G. Tarntair, J. B. Lin, K. H. Chen, L. C. Chen, *Electrochem. Solid-State Lett.* **2001**, *4(8)*, H15.
[14] W. K. Hong, K. H. Chen, L. C. Chen, F. G. Tarntair, K. J. Chen, J. B. Lin, H. C. Cheng, *Jpn. J. Appl. Phys.* **2001**, *40*, 3468.
[15] L. C. Chen, W. K. Hong, F. G. Tarntair, K. J. Chen, J. B. Lin, P. D. Kichambare, H. C. Cheng, K. H. Chen, *New Diamond Front. Carbon Technol.* **2001**, *11*, 249.
[16] L. Nilsson, O. Groening, C. Emmenegger, O. Kuettel, E. Schaller, L. Schlapbach, H. Kind, J.-M. Bonard, K. Kern, *Appl. Phys. Lett.* **2000**, *76*, 2071.
[17] M. Chhowalla, C. Ducati, N. L. Rupesinghe, K. B. K. Teo, G. A. J. Amaratunga, *Appl. Phys. Lett.* **2001**, *79*, 2079.
[18] W. Z. Li, S. S. Xie, L. X. Qian, B. H. Chang, B. S. Zou, W. Y. Zhou, R. A. Zhao, G. Wang, *Science* **1996**, *274*, 1701.
[19] Y. Chen, Z. L. Wang, J. S. Yin, D. J. Johnson, R. H. Prince, *Chem. Phys. Lett.* **1997**, *272*, 178.
[20] S. H. Tsai, C. W. Chao, C. L. Lee, H. C. Shih, *Appl. Phys. Lett.* **1999**, *74*, 3462.
[21] Y. C. Choi, Y. M. Shin, S. C. Lim, D. J. Bae, Y. H. Lee, B. S. Lee, *Appl. Phys. Lett.* **2000**, *76*, 2367.
[22] Y. Chen D. T. Shaw, *Appl. Phys. Lett.* **2000**, *76*, 2469.
[23] V. I. Merkulov, D. H. Lowndes, Y. Y. Wei, G. Eres, E. Voelkl, *Appl. Phys. Lett.* **2000**, *76*, 3555.
[24] C. Bower, W. Zhu, S. Jin, O. Zhou, *Appl. Phys. Lett.* **2000**, *77*, 830.
[25] C. J. Lee, D. W. Kim, T. J. Lee, Y. C. Choi, Y. S. Park, W. S. Kim, Y. H. Lee, W. B. Choi, N. S. Lee, J. M. Kim, Y. G. Choi, S. C. Yu, *Appl. Phys. Lett.* **1999**, *75*, 1721.
[26] H. Cui, O. Zhou, B. R. Stoner, *J. Appl. Phys.* **2000**, *88*, 6072.
[27] R. Andrews, D. Jacques, A. M. Rao, F. Derbyshire, D. Qian, X. Fan, E. C. Dickry, J. Chen, *Chem. Phys. Lett.* **1999**, *303*, 467.
[28] R. T. K. Baker, M. A. Braber, P. S. Harries, F. S. Feates, R. J. Waite, *J. Catal.* **1972**, *26*, 51.
[29] T. Baird J. R. Fryer, *Carbon* **1974**, *12*, 591.
[30] A. Oberlin, M. Endo, T. Koyama, *J. Cryst. Growth* **1976**, *32*, 335.

  1616-301X/02/1010-0692 $ 17.50+.50/0